Effect of temperature on the electrical and electromechanical properties of carbon nanotube/polypropylene composites

A Balam, Z Valdez-Nava, Vincent Bley, P Ayuso-Faber, H Carrillo-Escalante, A Castillo-Atoche, F Avilés

Effect of temperature on the electrical and electromechanical properties of carbon nanotube/polypropylene composites

A. Balam[1], Z. Valdez-Nava[2], V. Bley[2], P. Ayuso-Faber[1], H. Carrillo-Escalante[1], A. Castillo-Atoche[3], F. Avilés[1]*

[1] Centro de Investigación Científica de Yucatán A.C., Unidad de Materiales, Calle 43 No. 130 x 32 y 34, Col. Chuburná de Hidalgo, Mérida 97205, Yucatán, Mexico.

[2] LAPLACE, Université de Toulouse, CNRS, INPT, UPS, Toulouse, France.

[3] Facultad de Ingeniería, Universidad Autónoma de Yucatán, Av. Industrias No Contaminantes por Periférico Norte A.P. 150, Cordemex, Mérida 97000, Yucatán, Mexico.

*Correspondence: faviles@cicy.mx

Abstract

The effect of temperature on the electrical and electromechanical (piezoresistive) properties of composite films made of multiwall carbon nanotubes (MWCNTs) and polypropylene is investigated. The electrical response to temperature in alternating current (AC, i.e., thermoimpedance) showed higher sensitivity than in direct current (DC, thermoresistivity) and is influenced by frequency (f). The sensitivity factor in DC reached 1.07 %ºC^{-1}, while in AC at 100 Hz was 2.7 %C^{-1} for the impedance modulus for nanocomposites with 4 wt. % of MWCNTs. The electrical properties of the nanocomposites in AC investigated through broadband dielectric spectroscopy exhibited a resistive-capacitive behavior with a transition at $f \sim 10^4$ Hz. Temperature also showed a strong influence on the piezoresistive response of the nanocomposites, showing a 10 % increase in the piezoresistive sensitivity at 50 °C with respect to the response at 25 °C, and an important decrease in sensitivity at 100 °C for small (< 3 %) strains. The influence of temperature on the electrical and electromechanical responses investigated herein may assist in further developments of smart temperature-sensing materials, and in developing thermal compensation factors to properly calibrate piezoresistive/piezoimpedance responses for strain measurements.

Keywords: Temperature, direct current, alternating current, broadband dielectric spectroscopy, piezoresistivity, polymer nanocomposites.

1. Introduction

Multifunctionality and sensorial capabilities of smart polymeric nanocomposites based on carbon nanostructures have boosted research and development on nanostructured sensors and actuators. Of particular interest for these applications are carbon nanotubes (CNTs), given that their long aspect ratio and tubular morphology form percolated networks at very low filler concentrations [1,2]. The electrical properties of CNT/polymer nanocomposites depend on several factors, including the CNT content [1,3–5], properties of the polymeric matrix [1,4,6,7], dispersion state, and the processing method [8,9], among others. Temperature is another physical variable that may greatly affect the electrical conductivity of carbon nanostructured polymer nanocomposites [4,5,10–13]. The coupling phenomenon between the direct current (DC) electrical resistance (R) of the material and its temperature (T) is known as thermoresistivity. If the tests are conducted under alternating current (AC), the phenomenon is termed thermoimpedance [12–15]. In metallic materials, thermoresistivity has a positive linear response, that is, R increases linearly with increasing T. In semiconductors, R decreases nonlinearly with T [16]. For polymeric nanocomposites filled with CNTs, existent thermoresistive studies have reported both, an increase of R [3,4,10,17] (positive thermoresistivity) and a decrease of R [3,4,10,14] (negative thermoresistivity) with increasing T. The thermoresistive behavior of CNT/polymer nanocomposites depends on many factors such as the CNT content [3], the thermal expansion of the polymeric matrix [4], and sometimes the temperature interval (for nonlinear cases) [4,10], among others. Several mechanisms such as variable range hopping, electron tunneling, and the theory of the general effective medium help to understand the thermoresistive response [11,18,19]. However, the thermal expansion of the matrix is considered the main governing thermoresistive mechanism for polymeric nanocomposites with relatively low filler content (< 3 %) [3,4,10,17]. On other hand, thermoimpedance has been much less studied than thermoresistivity [12–14]. In this regard, the broadband dielectric spectroscopy (BDS) technique covers a wide frequency spectrum and a broad temperature range of the dynamic electrical response (AC) of a material [20]. Only a few works have reported the study of thermoimpedance of polymeric nanocomposites over a broad frequency range using BDS, identifying the dominance of interfacial polarization at low frequencies and the appearance of dipolar polarization effects at higher frequencies [13].

For sensing applications of smart materials, another important coupling phenomenon that occurs in nanocarbon-filled polymeric nanocomposites is the electric response to strain/stress. Such electromechanical coupling may manifest as a piezoresistive response for self-sensing of strain [7,17,21], or be used for structural health monitoring [22–24], as well as for the development of human/machine interfaces [25,26] and tactile sensors [27,28]. However, since polymer nanocomposites are sensitive to temperature, their piezoresistive response is also affected by temperature. In some instances, knowledge of the piezoresistive response to temperature can be used to compensate for temperature-dependent gauge factors or to tailor smart materials with a zero temperature coefficient of resistance [29,30]. Although there are a few reports on this topic [5,31–33], there is currently no systematic study that completely addresses these issues. Therefore, the present work systematically investigates the effect of temperature on the electrical and piezoresistive response of multiwall carbon nanotube (MWCNT)/polypropylene (PP) films fabricated through extrusion. Both thermoresistivity (DC) and thermoimpedance (AC) studies are conducted herein.

2. Materials and methods

2.1. Fabrication of nanocomposites

Multiwall carbon nanotubes (MWCNTs) were acquired from Cheaptubes Inc. (Grafton, VT, USA), produced by chemical vapor deposition with purity >95%, internal diameter between 4 and 10 nm, and external diameter close to 30 nm. The length of the MWCNTs was measured in previous works and fit to a log-normal distribution with an expected value of 2.6 μm [34]. Extrusion-grade homopolymer polypropylene (PP) from Formosa Plastics Co. (Livingston, NJ, USA), designated as Formolene® 1102KR, with a flow rate of 4 g/10 min was used as the polymeric matrix.

To produce ~200 μm thick MWCNT/PP nanocomposites, the MWCNTs were first dispersed into PP at three weight concentrations (3, 4, and 5 wt. %), using a batch mixer at 190 °C and 40 rpm for 10 min. Subsequently, the MWCNT/PP blends were extruded using a three-zone single-screw Brabender set to 190 °C with a screw speed of 30 rpm. The extruder was equipped with a 12 cm wide slot die with a die gap of 200 μm at 190 °C, to obtain the film morphology. To homogenize the thickness, the films were pulled-out from the extruder with a linear speed of 0.4 m/min using a Brabender take-off equipment with ~ 200 μm gap between rollers. This processing method yielded adequate dispersion of MWCNTs within the polymer

matrix. Scanning electron micrographies showing the state of dispersion of the MWCNTs within the PP are presented in section S.1 of the supplementary information.

2.2. Broadband dielectric spectroscopy characterization

Broadband dielectric spectroscopy (BDS) was carried out for the neat PP specimens (without CNTs) and for the CNT nanocomposites at three weight concentrations (3, 4 and 5 wt. %). The test specimens were 12 mm-diameter disk-shaped sections cut from the continuous films. Prior to electrical measurements, the specimens were metallized by sputtering circular 10 mm-diameter Au sections of ~40 nm thickness on each of the two major surfaces of the specimens. BDS measurements were performed using an Alpha-A broadband spectroscopic impedance analyzer from Novocontrol Technologies (Montabaur, Germany). The impedance modulus ($|Z|$) was obtained by calculating the ratio between the peak values of voltage (V_p) and current (I_p), and the phase offset between the sinusoidal alternating V_p and I_p signals corresponds to the phase angle (θ). BDS spectra were reported for $|Z|$ and θ. The nominal spectroscopic characterization was performed at 25 °C, by applying a root mean square voltage of 1 V through the thickness of the disk-shaped specimens, varying the frequency from 10^{-2} to 10^{7} Hz (10 frequency points per decade). Three specimens (replicates) were tested for each group of material.

To characterize the effect of temperature, BDS tests were also carried out on four replicates of 4 wt. % MWCNT/PP nanocomposites by varying the temperature from -100 °C to 100 °C, with steps of 15 °C. To determine the thermoimpedance response of the nanocomposites, the values of $|Z|$ and θ at different temperatures were extracted from the BDS spectra. Curves of $\Delta|Z|/|Z|_0$ and $\Delta\theta/\theta_0$, where $|Z|_0$ and θ_0 are $|Z|$ and θ at – 100 °C, were obtained as a function of T. Such curves were obtained for different frequencies of the applied voltage.

2.3. Characterization of the thermoresistive response

Thermoresistive characterization was performed for the 4 and 5 wt. % nanocomposites, since 3 wt. % nanocomposites exhibited a high electrical resistance, unsuitable for this test. The test specimens were 6.4 mm side squares (~ 200 μm thick) with a circular electrode of 6 mm diameter on each major surface of the specimen. Each thermoresistive test comprised 4 heating-cooling cycles, heating at 5 °C/min from room temperature (~ 25 °C) to ~ 100 °C, and subsequently cooling down at a similar rate. The electrical resistance (R) and the instantaneous temperature (T) of the specimen were monitored in situ. The temperature was

measured using a K-type thermocouple place on the top of the specimen. The thermocouple and the electrodes on the specimen were connected to a high-performance multifunction switch/meter Keysight 34980A (Santa Rosa, CA, USA) with a 34921A 40-channel multiplexer module. Measurements of R during the thermoresistive tests were carried out by the two-wire method, since the differences between this and the four-point probe method produced a root mean square global error of only 0.33 %, as documented in section S.2 of the supplementary information.

From the change in R with respect to the reference value at the beginning of each heating cycle (R_0), i.e. $\Delta R = R - R_0$, the fractional change of R ($\Delta R/R_0$) was calculated. Then, thermoresistive curves of $\Delta R/R_0$ against $\Delta T = T - T_0$ were plotted, where T_0 is the reference (room) temperature.

Since the $\Delta R/R_0$ vs. ΔT curves were nonlinear, to determine the temperature coefficient of resistance (or thermoresistive sensitivity, α_R), the heating sections of the cycles were divided into three temperature intervals. The first interval ranged from 0 °C ≤ ΔT ≤ 20 °C, the second 20 °C ≤ ΔT ≤ 55 °C, and the third one 55 °C ≤ ΔT ≤ 75 °C. For each temperature interval, α_R was determined from the slope of the $\Delta R/R_0$ vs. ΔT linear fit.

2.4. Piezoresistive characterization at different temperatures

Piezoresistive characterization was carried out at three temperatures, viz., 25 °C (room temperature), 50 °C and 100 °C, following a 5 replicate test plan. To perform the piezoresistive characterization, type III ASTM D638 standard specimens [35] downscaled 3:1 were cut from the extruded films, with the longest (axial) dimension aligned with the extrusion direction. The specimens were 82 mm long, ~ 200 µm thick, with 6.4 mm width in the narrow section and 9.7 mm in the widest (clamped) section. The specimens were subjected to uniaxial tensile loading until failure along the extrusion direction. Tensile loading was applied using a Shimadzu AGS-X universal testing machine with a 1 kN load cell, with a crosshead displacement speed of 1 mm/min. The crosshead displacement and load analog voltage signals were synchronized with the instantaneous electrical resistance measurements of the specimen (R) and recorded using a Keysight 34980A high-performance multifunction switch/meter equipment with a 34921A 40-channel multiplexer module. The two-wire method for measuring R was used since differences between the two-wire and four-wire resistance measurements were negligible. This is because the electrical resistance of the

films (10^4—10^5 Ω) is much higher than the contact resistance. Changes in electrical resistance ($\Delta R=R–R_0$) were calculated by subtracting the initial (mechanically unloaded) value (R_0) from the instantaneous value of R. The piezoresistive tests at 50 °C and 100 °C required a conditioning chamber. Such a thermally insulating chamber was made from thick PVC foam walls and controlled forced convection air from a heat gun (Baku 858L, Guangzhou, China). For piezoresistive testing, 15 min were waited before applying any load/strain, to stabilize the temperature and the electrical resistance of the specimen. This guarantees that changes in R are due to a change in strain (at constant temperature). The $\Delta R/R_0$ vs. ε (applied strain) response was plotted, with R_0 as the measured value of R prior to loading the specimen. Since the piezoresistive behavior was nonlinear, the piezoresistive curves were divided into two strain zones, viz., $\varepsilon \leq 0.8$ % and 1 % $\leq \varepsilon \leq 3$ %. A piezoresistive sensitivity factor (k) was determined for each strain zone from the slope of the piezoresistive linear fitting, for the three temperatures examined.

3. Results

3.1. Broadband impedance spectroscopy of nanocomposites

Representative BDS curves at 25 °C for neat PP and MWCNT/PP composites at 3, 4, and 5 wt. % are presented in Fig. 1. Figure 1a corresponds to the impedance modulus ($|Z|$) while Fig. 1b to the phase angle (θ). Figure 1a shows that for the neat polymer (PP) $|Z|$ decreases linearly with increasing frequency over the entire frequency range. The phase angle for PP (Fig. 1b) presents constant values close to −90° throughout the frequency interval (empty squares, which overlap with 3 wt.%). Such a behavior is typical of dielectric materials, in which their impedance response is influenced by polarization phenomena. The increase in polarization causes the impedance modulus to decrease with increasing frequency, and the phase angle to be constant at values close to −90°, indicating the strong contribution of the material's permittivity to the impedance [36,37]. As shown in both figures, the behavior of the nanocomposites with 3 wt. % is similar to that of the neat PP, with linearly decreasing values of $|Z|$ as f increases, and with values of θ fairly constant and close to − 90°. This behavior indicates that the MWCNT/PP composites at 3 wt.% have not yet reached electrical percolation, so their electrical properties are frequency-dependent and dominated by the properties of the polymer [38]. The behavior of the 4 wt. % nanocomposites is markedly different from that of PP and 3 wt. % nanocomposites, suggesting that the percolation

threshold lies between 3 and 4 wt. %. For 4 wt. %, $|Z|$ remains constant around 10^3 Ω (with changes < 0.5 %) for frequencies below 10^4 Hz, while for higher frequencies it decreases nonlinearly until values around 10^2 Ω.

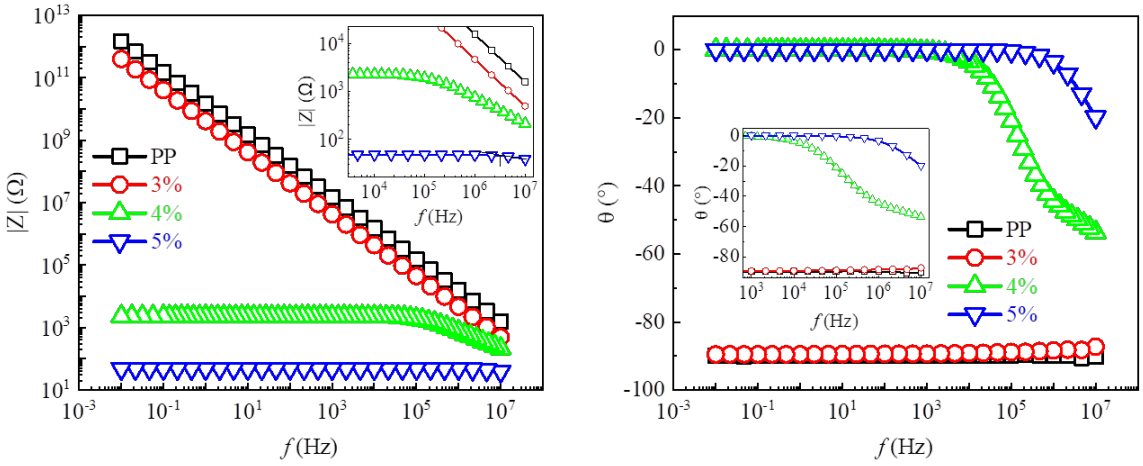

Fig. 1 Broadband impedance spectroscopy of neat PP and nanocomposites. a) $|Z|$, b) θ.

For 4 wt.% θ remains constant at small negative values (close to 0°) until frequencies between 10^3 and 10^4 Hz are reached. Beyond this range, θ decreases nonlinearly towards more negative values. A similar behavior was observed for 5 wt. % nanocomposites; however, the frequency-independent behavior is extended towards higher values of f for 5 wt.% composites. This frequency-independent behavior is associated with the dominance of the resistive component of the impedance, i.e., a response similar to the response expected in direct current (Ohmic behavior) [39,40]. Although the polarization phenomena are still present, these are masked by the conduction process [41]. The frequency-dependent behavior at high frequencies (> 10^4 Hz for 4 wt. % and > 10^6 Hz for 5 wt. %) indicates the increasing influence of interfacial polarization, due to the differences between the conductivities and permittivities of the polymer and CNTs [42]. The transition frequency where the frequency-independent zone changes to a frequency-dependent one has been named "critical frequency" (f_c) [43,44]. Herein, such a critical frequency was calculated from the intersection of straight lines corresponding to fittings of the frequency-dependent and frequency-independent regions of $|Z|$ in the BDS spectrum. The corresponding value of f_c determined for the 4 wt. % nanocomposites is 137.2 (± 5.6) kHz, while that for 5 wt. % is 4.6 (± 0.2) MHz.

For the case of θ, $\theta = 0$ indicates that the current and voltage are in phase (purely resistive response). Negative phase angles ($\theta < 0$) indicate that current leads voltage, storing charges

like in a capacitor [45]. According to this, the nanocomposites with 4 and 5 wt. % present a resistive-capacitive behavior (*RC*), with increasingly negative values of θ for higher frequencies. As for $|Z|$, the frequency at which the curve of θ becomes frequency-dependent shifts towards higher values for higher CNT content. In carbon-based nanocomposites, the nanostructures form percolative pathways where they are in contact with each other promoting electrical conduction, concomitant with their contact resistance. Likewise, the nanostructures or their agglomerates can be very close to each other, which favors electrical tunneling among them, and the formation of micro-capacitors. In this type of polymer composites, micro-capacitors are formed between two conductive nanostructures/agglomerates separated by a polymer dielectric layer [7,40]. This arrangement of resistors (*R*) and capacitors (*C*) plays a major role in the dielectric properties of the nanocomposite [46]. Based on this, nanocomposites behave as three-dimensional *RC* networks. In such networks, due to the limited current flow through the conducting regions, it is expected the presence of polarization phenomena and frequency dependence, due to the dielectric/polarizable behavior of the network [36]. The higher concentration of MWCNTs in the 5 wt. % nanocomposites favors a higher saturation of the percolative network and the formation of higher number of redundant conducting pathways, so the value of $|Z|$ is up to two orders of magnitude lower than for nanocomposites with 4 wt. %. The fact that the 5 wt. % nanocomposites showed a resistive (frequency-independent) dominance for frequencies two orders of magnitude higher than for the 4 wt. % ones indicates that in this case electron flow and CNT-to-CNT contact is favored for such a high CNT concentration, rather than the formation of micro-capacitors.

3.2. Effect of temperature in the impedance response

Fig. 2 shows the broadband impedance spectroscopy curves of the MWCNT/PP nanocomposites at 4 wt. %, characterized from -100 °C to 100 °C in steps of 15 °C. For all temperatures, it is observed that both $|Z|$ (Fig. 2a) and θ (Fig. 2b) show a similar trend to that for 25 °C (Fig. 1). However, in the region with resistive dominance ($f \leq 10^4$ Hz) $|Z|$ increases with increased temperature (~120 % increment from -100 °C to 100 °C, see inset, where -100 °C corresponds to the lower curve). At higher frequencies ($f > 10^4$ Hz), $|Z|$ converges to similar values of $|Z|$ regardless of T, exhibiting only small differences among all curves (~ 10 % for $f = 10^7$ Hz). θ shows a decrease towards more negative values as the temperature

increases (see inset in Fig. 2b, where -100 °C is the top curve), which is significantly more marked for $f > 10^3$ Hz. However, the values of θ are less sensitive to T than to $|Z|$, i.e., they are not largely different for all temperatures tested. The differences between θ at $T = -100$ °C and T=100 °C slightly increase with f, showing a difference of ~ 4 % at 10^7 Hz.

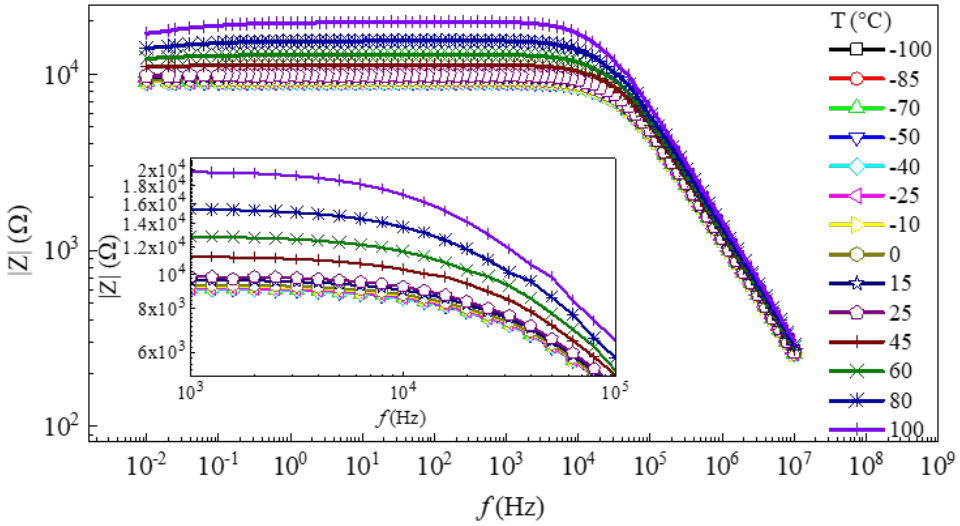

a)

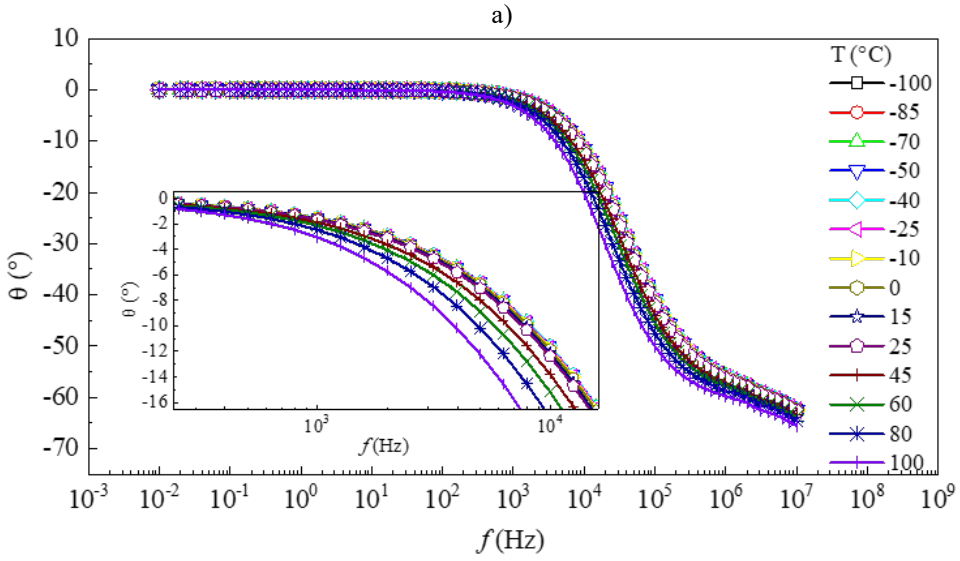

b)

Fig. 2 Broadband impedance spectroscopy of nanocomposites at 4 wt.%. a) $|Z|$, b) θ.

The values of the critical frequency separating the frequency-independent from the frequency-dependent regions (f_c) are influenced by temperature, as seen in Fig. 3a. They present fairly constant values with only small fluctuations between −100 °C and 15 °C, and decrease for T >15 °C. To further depict the effect of temperature, Fig. 3b presents the behavior of $|Z|$ at a selected frequency (100 Hz, labeled $|Z|_{100}$) as a function of temperature. $|Z|_{100}$ remains constant or with small changes (< 1%) at temperatures below 0 °C. Then, it

increases nonlinearly until reaching 100 °C. This increase of impedance modulus at high temperatures can be related to the thermomechanical properties of the MWCNT/PP composites. When the polymer expands due to temperature rise, the MWCNTs dispersed in the matrix are dragged by the polymer chains, causing an increase in the CNT-to-CNT distance [11]. Since the coefficient of thermal expansion of PP is quite high, 18×10^{-5} $°C^{-1}$ [47], this effect should be particularly relevant for PP and other polymers with high thermal expansion. When PP thermally expands, existent contact and tunneling joints between CNTs become disrupted and also the effective CNT volume fraction decreases [4,11,17]. In AC, in addition to these factors, the thermoimpedance response is associated to the frequency and the density of micro-capacitors formed by the CNTs and their agglomerates, separated by a polymer layer [40].

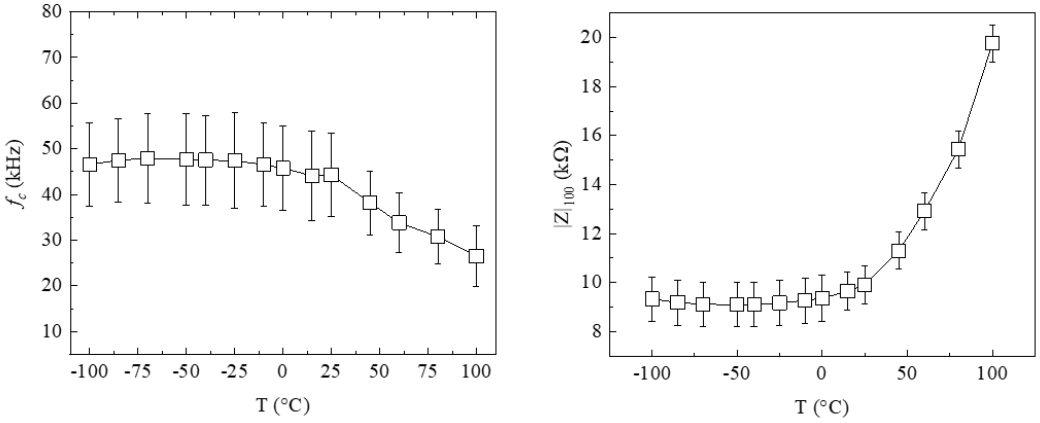

Fig. 3 Effect of temperature on the electrical impedance of the 4 wt. % MWCNT/PP nanocomposites. a) Critical frequency as a function of temperature, b) impedance modulus at 100 Hz vs. *T*.

The polymer thermal expansion also changes the network configuration and polymer spacing of such micro-capacitors. The thermal expansion of the polymer causes the CNTs and their agglomerates to separate in all three dimensions, so the resistive component of the impedance is expected to increase with increasing temperature, see Fig. 3b. The separation of the CNTs and their agglomerates that were originally in contact may promote the formation of a larger number of micro-capacitors [40]. Higher number of micro-capacitors increases the susceptibility of the material to polarization effects with increasing temperature [45,48], causing a decrease in the critical frequency for higher temperatures, as seen in Fig. 3a. For frequencies lower than f_c, polarization effects so the majority of the micro-capacitors may behave like open circuits [42,44,48]. In this sense, it has been reported that MWCNT/PP nanocomposites below the electrical percolation threshold behave as highly polar dielectrics

at temperatures below 80 °C, and present dielectric relaxation effects for $f > 1$ MHz [13]. According to Olariu *et al*. [13], at high temperatures these materials behaved as conductors, leading to the disappearance of the relaxation phenomenon [13]. In the case of the nanocomposites studied herein, the temperature effect on f_c is observed from 15 °C and above, which indicates that from this temperature the spacing between CNT agglomerates and their mobility is sufficient to promote thermal activation effects.

To further study the effect of temperature and frequency on the impedance response of the nanocomposites, Fig. 4 presents representative thermoimpedance curves at 100 Hz (below f_c, Fig. 4a) and at 100 kHz (above f_c, Fig. 4b), extracted from the BDS curves of Fig. 2. For these curves $|Z|_0$ is the value of $|Z|$ at -100 °C. Similar thermoimpedance curves for 10 Hz and 1 kHz are presented in section S.3 of the supplementary information.

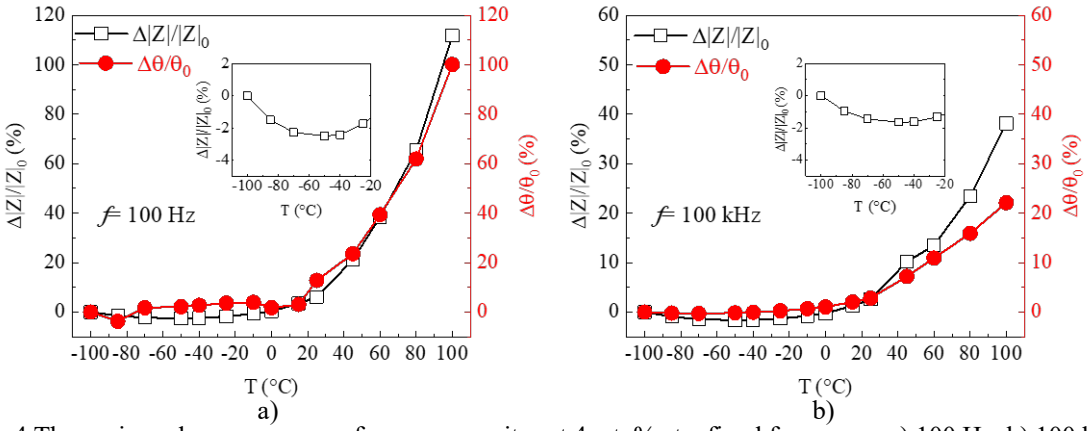

Fig. 4 Thermoimpedance response of nanocomposites at 4 wt. % at a fixed frequency. a) 100 Hz, b) 100 kHz.

For both frequencies examined in Fig. 4, $\Delta|Z|/|Z|_0$ shows a slight decrease of up to 3% (negative thermoimpedance) when the temperature increases from −100 °C to −45 °C, as indicated in the insets of Fig. 4. In the range of −45 °C < T < 25 °C, $\Delta|Z|/|Z|_0$ increases moderately until ~ 2.5 %. For $T \geq 25$ °C, the rate of increase of $\Delta|Z|/|Z|_0$ with temperature increases nonlinearly until 100 °C. At 100 Hz (Fig. 4a), the maximum value of $\Delta|Z|/|Z|_0$ at 100 °C was ~120%, while for 100 kHz (Fig. 4b) the maximum $\Delta|Z|/|Z|_0$ was ~40 %. The behavior of $\Delta\theta/\theta_0$ is qualitatively similar to that of $\Delta|Z|/|Z|_0$ but attains lower magnitudes. At f= 100 Hz $\Delta\theta/\theta_0$ slightly decreases from −100 to −40 °C; thereafter, there is a slight increase (< 3 %) up to 25°C. Finally, from 25 °C to 100 °C $\Delta\theta/\theta_0$ increases nonlinearly, showing maximum values (at 100 °C) of ~100 % (Fig. 4a). At 100 kHz (Fig. 4b), the maximum $\Delta\theta/\theta_0$ was ~20%. As observed in Fig. 4, beyond the kHz range, the sensitivity to temperature decreases with increased frequency. Such behavior is attributed to the incremental

contribution of the polarization phenomena with increased frequency, as will be further explained.

Since the thermoimpedance curves of Fig. 4 are nonlinear, termoimpedance sensitivity for $|Z|$($\alpha_{|Z|}$) and for θ (α_θ) were obtained from linear fittings in four regions, as indicated in the inset of Fig. 5. As observed in Fig. 5, both sensitivities ($\alpha_{|Z|}$ and α_θ) increase as the temperature increases. In the interval $-100\ °C \leq T \leq -40\ °C$, $\alpha_{|Z|}$ and α_θ are very small and negative, while for $T > -40\ °C$ all sensitivity coefficients are positive. This is because at −40 °C there is a transition from negative to positive thermoimpedance, as observed in the insets of Fig. 4. This temperature coincides with the glass transition temperature (T_g) of the nanocomposite determined by differential scanning calorimetry (DSC), as discussed in section S.4 of supplementary information.

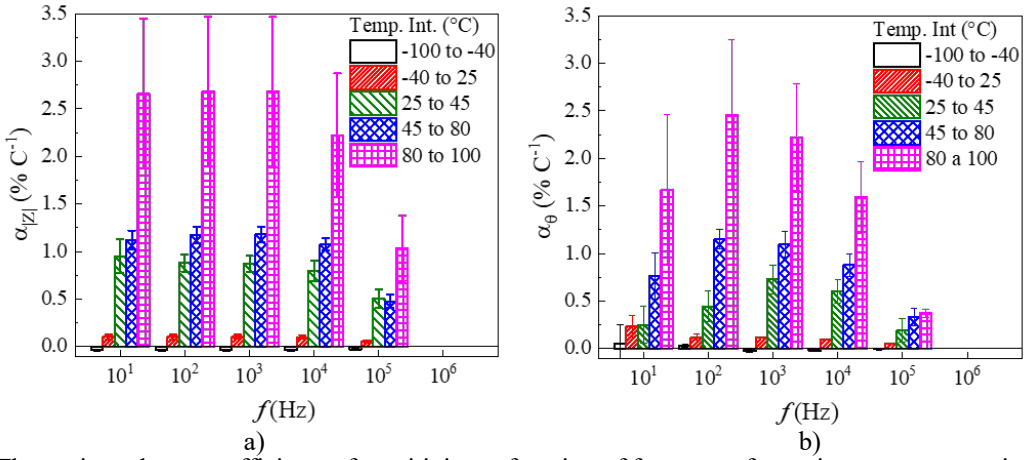

Fig. 5 Thermoimpedance coefficients of sensitivity as function of frequency for various temperature intervals. a) $\alpha_{|Z|}$, b) α_θ.

It is known that for temperatures below T_g, the mobility of the polymeric chains in the amorphous regions of PP and that of the CNTs located within such amorphous regions is restricted [36]. Thus, at low temperatures (-100 to -40 °C), the electrical response to temperature is expected to be dominated by phenomena that promotes a negative temperature dependence [4,49], such as the intrinsic thermoresistivity of CNTs [50], tunneling effects induced by AC fluctuations [51] and/or temperature-assisted variable range hopping [18]. Research on CNT/polyester nanocomposites at concentrations above percolation has pointed out that thermoimpedance can be dominated by the same governing mechanisms than thermoresistance (DC) [41], as long as they are below f_c. In this sense, it is considered that the polarization phenomena cause the impedance modulus and phase angle to decrease

towards more negative values for θ. With the volumetric expansion of the polymer caused by temperature rise, the number of micro-capacitors is expected to increase as well. This may justify the observed experimental behavior of the increase in sensitivity with increased temperature and the decrease for very high frequencies (>kHz). For frequencies above the kHz range, the mechanisms governing the increase in $|Z|$ and the decrease in θ with temperature (see Fig. 2) may compete, limiting the synergy observed in $\alpha_{|Z|}$ and α_{θ}.

3.3. Thermoresistive response

Figure 6 shows the (DC) cyclic thermoresistive response (fractional change of electrical resistance as a function of temperature change) of the MWCNT/PP nanocomposites at 4 wt. % and 5 wt. %. The first cycle (cycle 0) was not considered for the analysis to eliminate any potential thermal history of the nanocomposites [4,10].

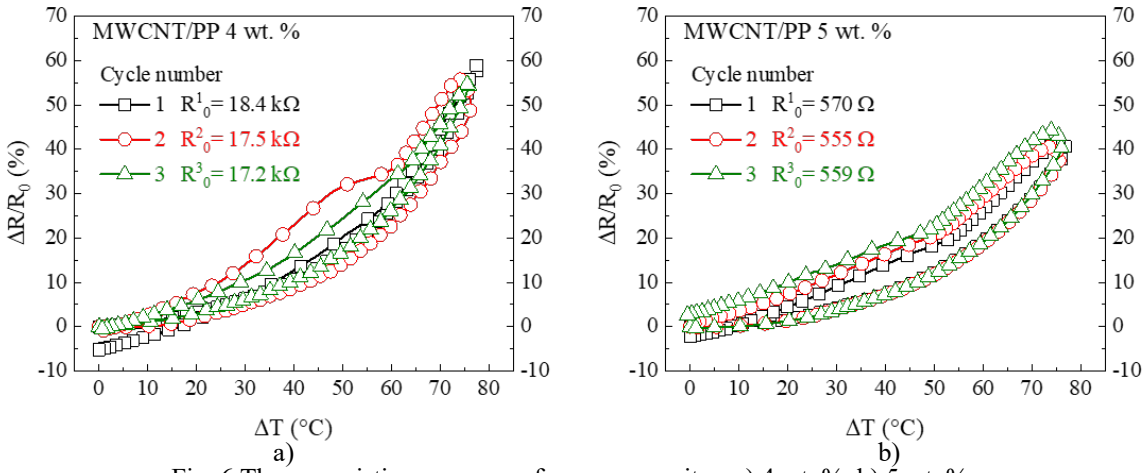

Fig. 6 Thermoresistive response of nanocomposites. a) 4 wt. %, b) 5 wt. %.

As is observed in Fig. 6, a nonlinear response is observed for both nanocomposites. To reproduce this kind of curves, a nonlinear thermoresistive model is needed. For example, a model based on the product of a power law and an exponential function was reported in [4]. However, from such a nonlinear model it is not strictly possible to determine a linear sensitivity factor, such as the temperature coefficient of resistance (*TCR*). Thus, for practical analysis purposes, the thermoresistive curves were divided herein into the three zones indicated in section 2.3 for calculation of the *TCR* (α_R), as a metric of thermoresistive sensitivity. The sensitivities calculated in this way are listed in Table 1. For 4 wt.% nanocomposites (Fig. 6a), the maximum values of $\Delta R/R_0$ at 100 °C reach ~ 57 %, while for 5 wt. % (Fig. 6b) reach ~ 42 %. The thermoresistive response of CNT/polymer nanocomposites at low CNT concentration is strongly influenced by the thermal expansion

of the polymeric matrix [11]. Upon thermal expansion of the polymer, the tunneling effect between CNTs and the change in the effective volume fraction of CNTs in the nanocomposite play a paramount role in such a thermoresistive response.

Table. 1 Temperature coefficients of resistance (thermoresistive sensitivity) in three temperature ranges.

MWCNT content (wt. %)	α_R **(% °C^{-1})**		
	0 ≤ ΔT ≤ 20 °C	**20 °C ≤ ΔT ≤ 55 °C**	**55 °C ≤ ΔT ≤ 75 °C**
4	0.08 (± 0.04)	0.4(± 0.06)	1.07 (± 0.23)
5	0.11 (± 0.02)	0.33 (± 0.03)	0.86 (± 0.11)

For the case of MWCNT/PP nanocomposites, the coefficient of thermal expansion of PP is around 18×10^{-5} C^{-1} [47], which is a considerably high value even among polymers. During heating, the matrix expands increasing the inter-CNT distances, and consequently the electrical resistance increases. The nonlinear response is attributed to the dominance of the tunneling mechanism induced by thermal expansion, as reported previously [4,10,17]. In PP nanocomposites the CNTs preferentially allocate within the amorphous region of the polymer [52,53], so the crystalline sections of PP hinder direct contact between CNTs during thermal expansion.

The sensitivities presented in Table 1 are higher than those reported in the literature for other thermoplastic matrices such as polysulfone [7] and thermosetting matrices such as vinyl ester resin [10]. Such a thermoresistive response is highly influenced by the thermomechanical properties of the PP matrix, mainly the coefficient of thermal expansion [4,11].

To compare the thermoresistive/thermoimpedance response in AC and DC, Fig. 7 summarizes the average and one standard deviation of the sensitivity coefficients determined in DC (α_R) and AC ($\alpha_{|Z|}$ and α_θ) at 100 Hz and 100 kHz. The subscript "100" refers to f = 100 Hz, while the subscript "100k" refers to f = 100 kHz. The values of $\alpha_{|Z|}$ and α_θ were determined from the response of $\Delta|Z|/|Z|_0$ and $\Delta\theta/\theta_0$, considering $|Z|_0$ and θ_0 as the corresponding values at 25 °C. Higher sensitivity coefficients are observed in AC, especially for $\alpha_{|Z|}$. In DC, the thermoresistive response relies only on the electrical resistance (governed by tunneling and inter-CNT contact resistance). For AC, the concomitant contributions from the electrical resistance (CNT separation distance) and reactance (formation of CNT-

polymer-CNT microcapacitors) seems to be synergistic and yield higher sensitivities than for DC, as long as the frequency range is moderate (below a few kHz).

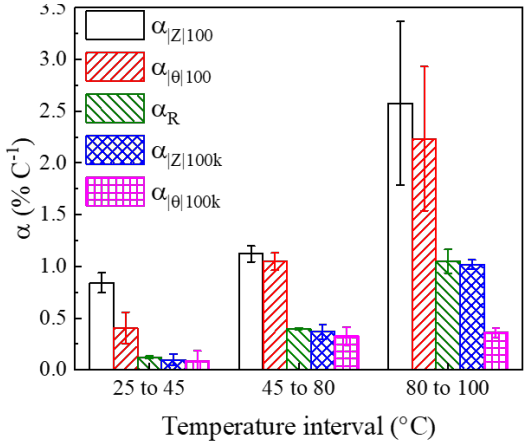

Fig. 7 Temperature coefficients of resistance/impedance in DC (α_R) and AC ($\alpha_{|Z|}$ and α_θ) at f= 100 Hz (100 labels) f= 100 kHz (100k labels) for three temperature intervals.

In the thermoimpedance response at low or moderate frequencies, the resistive and the permittive/capacitive components concur during the thermal excitation, yielding higher sensitivities than in DC. On the other hand, at frequencies higher than f_c (such as 100 kHz), the charges accumulated within the micro-capacitors yield a decrease in impedance [36,37]. Such an effect has a contrary trend to the effect that produces the electrical resistance on the thermoimpedance, yielding an effective decrease in sensitivity with respect to f = 100 Hz, as observed in Fig. 7.

3.4. Effect of temperature on the piezoresistive response

Figure 8 shows representative mechanical (σ vs. ε) and piezoresistive ($\Delta R/R_0$ vs. ε) responses of the 4 wt. % MWCNT/PP nanocomposites at 25 °C (Fig. 8a), 50 °C (Fig. 8b) and 100 °C (Fig. 8c). For the three temperatures examined, the stress-strain response exhibited linear behavior for small strains (elastic regime), followed by yielding and viscoelastic/viscoplastic creep. However, the strain level at which these events occurred varied depending on the test temperature (see the numerical scales of the horizontal axis, ε). The average elastic modulus (E) showed a decrease from E=1.32 GPa at 25 °C to E= 840 MPa at 50 °C, and even more (E= 42 MPa) at 100 °C.

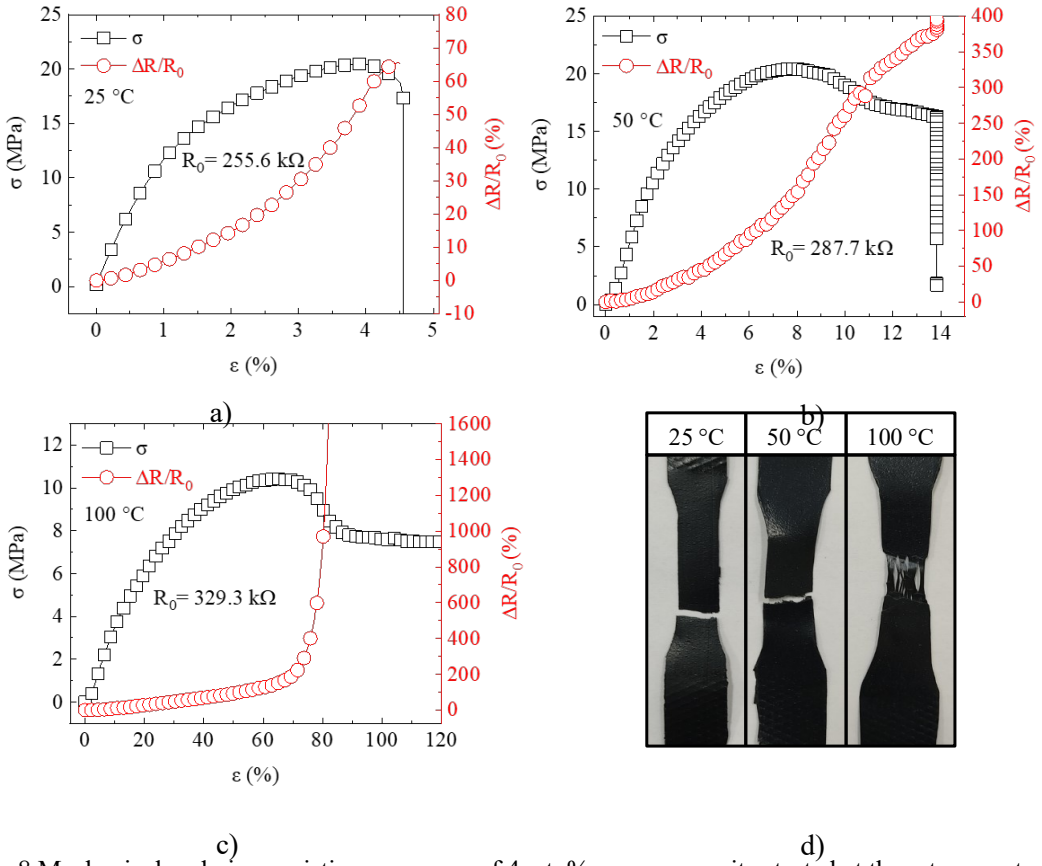

Fig. 8 Mechanical and piezoresistive responses of 4 wt. % nanocomposites tested at three temperatures. a) 25 °C, b) 50 °C, c) 100 °C, d) photographs of the failed specimens.

According to the 0.1% shift yield criterion [35], yielding occurs at ε_y = 1.15 % for 25 °C, ε_y = 2.5 % for 50 °C, and ε_y ~ 5.7 % for 100 °C. At 25 °C and 50 °C, failure of the specimens occurred due to marked breakdown of intermolecular forces. However, for 50 °C, crazing was observed prior to final failure. On the other hand, at 100 °C crazing was more marked and continued until both parts of the specimen were only connected by a few polymeric fibrils, as shown in Fig. 8d. The most marked effect of the temperature in the mechanical response is observed in the ultimate strain (ε_{max}), as indicated in Table 2.

Table. 2 Mechanical properties of 4 wt. % nanocomposites tested at three constant temperatures.

***T* (°C)**	***E* (GPa)**	**σ_y (MPa)**	**ε_y (%)**	**ε_{max} (%)**
25	1.32 (± 0.08)	11.9 (± 0.03)	1.15 (± 0.03)	4.5 (± 0.2)
50	0.84 (± 0.3)	14.3 (± 0.8)	2.5 (± 0.1)	15.5 (± 2.6)
100	0.04 (± 0.01)	2.5 (± 1.2)	5.7 (± 1.1)	> 200

At 100 °C the specimens creeped without failure until ε > 200% (only up to ε = 120 % is shown). Crazing is one of the most common failure modes reported for nanocomposites with semi-crystalline matrices such as PP [54]. At high temperatures, the larger mobility of the polymeric chains favors the formation of crazes. For large strains, the stress redistributes among the fibrils that remain connected (see Fig. 8d at 100 °C), so the load-bearing capacity (stress) decreases but the material is still able to deform visco-plastically. In this regard, DSC (presented in section S.4 of the supplementary information) measured the glass transition (T_g = −40 °C) and melting temperatures (T_m= 169.5 °C) of the polymer. Thus, the temperature range explored is between T_g and T_m, i.e., when the polymer is in a rubbery state [55]. This region is characterized by the reduction in the mechanical properties due to the high mobility of the amorphous regions of the polymer, while the crystalline regions still maintain their defined conformation and packaging. Figure 9a shows a comparative plot of the piezoresistive response at the three temperatures examined in the strain interval $0 \leq \varepsilon \leq 3$ %.

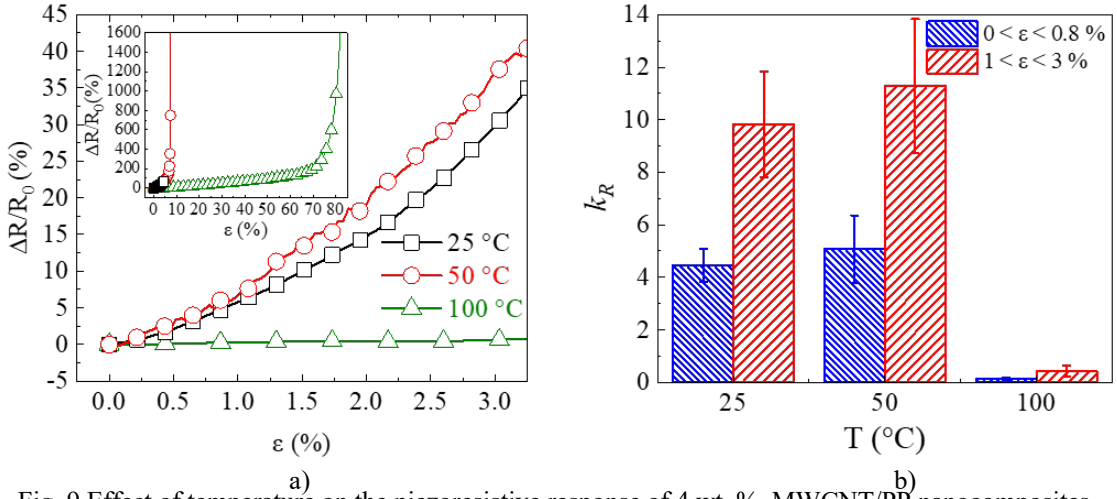

Fig. 9 Effect of temperature on the piezoresistive response of 4 wt. %. MWCNT/PP nanocomposites. a) Piezoresistive response at different temperatures, b) piezoresistive sensitivity coefficients (k_R).

As seen from this figure, the temperature has an important influence on the piezoresistive response of the MWCNT/PP nanocomposites. In this regard, dynamic mechanical analysis (DMA, presented in section S.4 of the supplementary information) showed that the storage modulus steeply decreases from 25 C to 100 C. In the same temperature interval, the loss modulus showed an increase from 25 °C to 80 °C, related to the high mobility of the polymeric chains and energy dissipation [55]. For T>80 °C the behavior of the damping factor of the DMA response (section S.4 of the supplementary information) indicates the

presence of α-relaxations, and the increase of segmental mobility of the crystalline regions of the polymer, caused by the high mobility of the amorphous regions [56].Such a structural phenomenon has a strong effect on the piezoresistive response, because the values of $\Delta R/R_0$ were considerably different for each test temperature. Bear in mind that the maximum values of $\Delta R/R_0$ were not achieved at the same strain levels, since the stiffness and deformation capability of each group of nanocomposites were strongly dependent on temperature, see Fig. 8. Table 3 presents a summary of the $\Delta R/R_0$ values reached at specific strains for the three test temperatures. Keep in mind that these values cannot be strictly used to define piezoresistive gauge factors, since they correspond to irreversible strains.

Table. 3 $\Delta R/R_0$ values reached at different strain levels for the three test temperatures.

Temperature (°C)	**$\Delta R/R_0$ (%)**			
	ε= 3 %	**ε= 4.5 %**	**ε= 15 %**	**ε= 80 %**
25	30 (± 1.5)	67 (± 1.2)	-	-
50	37 (± 3.5)	75 (± 4.1)	380 (± 10.8)	-
100	1.5 (± 0.2)	8.2 (± 1.4)	19 (± 2.3)	> 1500

In Fig. 8b it is observed that at 50 °C there was a slight increase in the piezoresistive sensitivity compared to 25 °C, while at 100 °C the sensitivity at $\varepsilon \leq 3$ % decreased significantly. However, when tested at 100 °C, considerably higher values of $\Delta R/R_0$ are reached at higher strain levels. These large strain regions, however, are irreversible and thus the response cannot be deemed piezoresistivity [57]. Therefore, to quantify the effect of temperature on the piezoresistive sensitivity of the nanocomposites, Fig. 9b shows the average and one standard deviation values of the piezoresistive sensitivity (gauge factor, k_R) obtained for each temperature examined, split into two small strain intervals. For both strain intervals, an increase in sensitivity is observed at 50 °C (increase of ~ 9 % for $\varepsilon \leq 0.8$ % and of ~ 15 % for 1 % $\leq \varepsilon \leq 3$ %, with respect to the test at 25 °C). At 100 °C, the sensitivity in this strain range dropped dramatically (decrease of ~ 97 % for $\varepsilon \leq 0.8$% and of ~ 95 % for 1% $\leq \varepsilon \leq 3$%, with respect to 25 °C). A similar behavior has been reported by Verma *et al.* [5] for MWCNTT/PP nanocomposites obtained by additive manufacturing. Regarding the higher sensitivity observed at 50 °C, according to the DMA conducted herein (section S.4 of supplementary information) at 50 °C the storage modulus decreases 20 % with respect to the value at 25 °C. The loss modulus increases in an important fashion from 40 °C to 70 °C, indicating high mobility of the polymer chains at 50 °C. Such a high molecular mobility

facilitates the motion and structural changes of the percolative network of MWCNTs during straining/loading [11]. This yields higher piezoresistive sensitivity at 50 °C than at 25 °C. On the other hand, according to the loss modulus and damping ratio measured by DMA, at 100 °C the amorphous regions of the polymer experience higher mobility than at 50 °C and the segmental mobility of the crystalline regions increases as well [56]. This segmental mobility could promote the MWCNTs to enter the zones between the crystallites, causing low mobility of the MWCNTs within the polymer during strain application. This, in turn, would yield only small structural changes in the CNT percolative network at this high temperature, which explains the limited piezoresistive sensitivity observed at 100 °C.

4. Conclusions

The effect of temperature on the electrical response of MWCNT/PP composites under alternating current (AC) and direct current (DC) has been investigated. The thermoimpedance response was compared to the thermoresistive one, and the effect of temperature on the piezoresistive response was also investigated. The nanocomposites were manufactured by a film extrusion process at three MWCNT weight concentrations (3, 4 and 5 wt. %). Broadband dielectric impedance spectroscopy of the nanocomposites revealed a resistive-capacitive behavior, with electrical percolation between 3 and 4 wt. %. For percolated nanocomposites, the impedance transition from a frequency-independent (Ohmic) behavior to a frequency-dependent one at higher frequencies occurred at a critical frequency, where the interfacial polarization phenomena became prominent. This critical frequency was ~ 10^4 Hz for 4 wt. %, ~ 10^6 Hz for 5 wt. %, and it slightly decreased with increased temperature.

The electrical response to temperature in AC (thermoimpedance) of the 4 wt. % nanocomposites showed a dependence on both, temperature and frequency. The thermoimpedance and thermoresistive sensitivities increased as the temperature increased. Higher sensitivities were found in AC than in DC, for frequencies below the kHz range. The highest sensitivity (2.7 %ºC^{-1}) was found for the impedance modulus at 100 Hz in the 80 to 100 °C range. Temperature also showed a strong influence on the piezoresistive response of the nanocomposites. Structural changes of the CNT network driven by temperature play a major role in the piezoresistive response of the nanocomposites. For the same strain range ($1 \leq \varepsilon \leq 3$ %), the average piezoresistive sensitivity at 50 °C (11.3) was ~ 15 % higher than that

at 25 °C (9.82), while at 100 °C was considerably smaller (0.41). The influence of temperature on the electrical and electromechanical responses of polymeric nanocomposites are topics of great interest for the development of smart self-sensing materials. Proper knowledge of such responses may assist not only in further developments of smart temperature-sensing materials, but also in developing thermal compensation factors to properly calibrate piezoresistive/piezoimpedance responses for strain measuring devices.

Acknowledgments

This research was supported by the US Office of Naval Research Global (ONRG) under award number N62909-19-1-2119. The authors acknowledge the valuable support of Miguel A. Rivero Ayala during composite manufacturing. Authors are also thankful to Carlos Medina for his help in the thermoresistive characterization, and to César Pérez and Gabriel Arana for their support during piezoresistive testing. Technical assistance of Céline Combettes at LAPLACE-UPS is greatly appreciated.

Conflict of interest

The authors declare no conflict of interest.

References

[1] Bauhofer W and Kovacs J Z 2009 A review and analysis of electrical percolation in carbon nanotube polymer composites *Compos. Sci. Technol.* **69** 1486–98

[2] Abdulhameed A, Wahab N Z A, Mohtar M N, Hamidon M N, Shafie S and Halin I A 2021 Methods and Applications of Electrical Conductivity Enhancement of Materials Using Carbon Nanotubes *J. Electron. Mater.* **50** 3207–21

[3] Cen-Puc M, Pool G, Oliva-Avilés A I, May-Pat A and Avilés F 2017 Experimental investigation of the thermoresistive response of multiwall carbon nanotube / polysulfone composites under heating-cooling cycles *Compos. Sci. Technol.* **151** 34–43

[4] Balam A, Cen-Puc M, May-Pat A, Abot J L and Avilés F 2020 Influence of polymer matrix on the sensing capabilities of carbon nanotube polymeric thermistors *Smart Mater. Struct.* **29** 015012

[5] Verma P, Schiffer A and Kumar S 2021 Thermo-resistive and thermo-piezoresistive sensitivity of carbon nanostructure engineered thermoplastic composites processed via additive manufacturing *Polym. Test.* **93** 106961

[6] Gong S, Zhu Z H and Li Z 2017 Electron tunnelling and hopping effects on the temperature coefficient of resistance of carbon nanotube/polymer nanocomposites *Phys. Chem. Chem. Phys.* **19** 5113–20

[7] Avilés F, Oliva-Avilés A I and Cen-Puc M 2018 Piezoresistivity, Strain, and Damage Self-Sensing of Polymer Composites Filled with Carbon Nanostructures *Adv. Eng. Mater.* **20** 1701159

[8] Nanni F, Mayoral B L, Madau F, Montesperelli G and McNally T 2012 Effect of MWCNT alignment on mechanical and self-monitoring properties of extruded PET-MWCNT nanocomposites *Compos. Sci. Technol.* **72** 1140–6

[9] Zhao K, Li S, Huang M, Shi X, Zheng G, Liu C, Dai K, Shen C, Yin R and Guo J Z 2019 Remarkably anisotropic conductive MWCNTs/polypropylene nanocomposites with alternating microlayers *Chem. Eng. J.* **358** 924–35

[10] Lasater K L and Thostenson E T 2012 In situ thermoresistive characterization of multifunctional composites of carbon nanotubes *Polymer* **53** 5367–74

[11] Cen-Puc M, Oliva-Avilés A I and Avilés F 2017 Thermoresistive mechanisms of carbon nanotube/polymer composites *Phys. E* **95** 41–50

[12] Macutkevic J, Kuzhir P P, Paddubskaya A G, Banys J, Maksimenko S A, Stefanutti E, Micciulla F and Bellucci S 2013 Broadband dielectric/electric properties of epoxy thin films filled with multiwalled carbon nanotubes *J. Nanophotonics* **7** 073593

[13] Olariu M, Scarlatache V-A, Niagu A, Ursache S and Ciobanu R C 2012 The influence of frequency and temperature upon dielectric behavior of polypropylene reinforced with multi-walled carbon nanotubes (MWCNTs) *2012 13th International Conference on Optimization of Electrical and Electronic Equipment (OPTIM)* (IEEE) pp 287–92

[14] Kim B, Lee J and Yu I 2003 Electrical properties of single-wall carbon nanotube and epoxy composites *J. Appl. Phys.* **94** 6724

[15] Bukreev D A, Derevyanko M S, Moiseev A A and Semirov A V 2020 Effect of tensile stress on cobalt-based amorphous wires impedance near the magnetostriction compensation temperature *J. Magn. Magn. Mater.* **500** 166436

[16] Kittel C 2005 *Introduction to Solid State Physics* (Hoboken, NJ: John Wiley & Sons, Ltd)

[17] Tjong S C, Liang G D and Bao S P 2007 Electrical behavior of polypropylene/multiwalled carbon nanotube nanocomposites with low percolation threshold *Scr. Mater.* **57** 461–4

[18] Yosida Y and Oguro I 1998 Variable range hopping conduction in multiwalled carbon nanotubes *J. Appl. Phys.* **83** 4985–7

[19] Simmons J G 1963 Generalized formula for the electric tunnel effect between similar electrodes separated by a thin insulating film *J. Appl. Phys.* **34** 2581–90

[20] Poplavko Y 2021 *Dielectric Spectroscopy of Electronic Materials* (Sawston, UK: Elsevier)

[21] Yan T, Wu Y, Yi W and Pan Z 2021 Recent progress on fabrication of carbon nanotube-based flexible conductive networks for resistive-type strain sensors *Sensors Actuators A Phys.* **327** 112755

[22] Tang Z-H, Li Y-Q, Huang P, Wang H, Hu N and Fu S-Y 2021 Comprehensive evaluation of the piezoresistive behavior of carbon nanotube-based composite strain sensors *Compos. Sci. Technol.* **208** 108761

[23] Coppola B, Di Maio L, Incarnato L and Tulliani J-M 2020 Preparation and Characterization of Polypropylene/Carbon Nanotubes (PP/CNTs) Nanocomposites as Potential Strain Gauges for Structural Health Monitoring *Nanomaterials* **10** 814

[24] Ding S, Wang X, Qiu L, Ni Y, Dong X, Cui Y, Ashour A, Han B and Ou J 2023 Self-Sensing Cementitious Composites with Hierarchical Carbon Fiber-Carbon Nanotube Composite Fillers for Crack Development Monitoring of a Maglev Girder *Small* **19** 2206258

[25] Yiu C, Wong T H, Liu Y, Yao K, Zhao L, Li D, Hai Z, Zheng H, Wang Z and Yu X 2020 Skin-Like Strain Sensors Enabled by Elastomer Composites for Human–Machine Interfaces *Coatings* **10** 711

[26] Dai H and Thostenson E T 2019 Large-Area Carbon Nanotube-Based Flexible Composites for Ultra-Wide Range Pressure Sensing and Spatial Pressure Mapping *ACS Appl. Mater. Interfaces* **11** 48370–80

[27] Sun X, Wang C, Chi C, Xue N and Liu C 2018 A highly-sensitive flexible tactile sensor array utilizing piezoresistive carbon nanotube–polydimethylsiloxane composite *J. Micromechanics Microengineering* **28** 105011

[28] Yang T, Xie D, Li Z and Zhu H 2017 Recent advances in wearable tactile sensors: Materials, sensing mechanisms, and device performance *Mater. Sci. Eng. R Reports* **115** 1–37

[29] Chu K, Lee S-C, Lee S, Kim D, Moon C and Park S-H 2015 Smart conducting polymer composites having zero temperature coefficient of resistance *Nanoscale* **7** 471–8

[30] Gao W, Zhang Z, Zhang Y, Ma B, Luo J, Deng J and Yuan W 2020 Efficient carbon nanotube/polyimide composites exhibiting tunable temperature coefficient of resistance for multi-role thermal films *Compos. Sci. Technol.* **199** 108333

[31] Sanli A, Benchirouf A, Müller C and Kanoun O 2017 Piezoresistive performance characterization of strain sensitive multi-walled carbon nanotube-epoxy nanocomposites *Sensors Actuators A Phys.* **254** 61–8

[32] Zhou P, Cao W, Liao Y, Wang K, Yang X, Yang J, Su Y, Xu L, Zhou L, Zhang Z and Su Z 2020 Temperature effect on all-inkjet-printed nanocomposite piezoresistive sensors for ultrasonics-based health monitoring *Compos. Sci. Technol.* **197** 108273

[33] Haghgoo M, Ansari R, Hassanzadeh-Aghdam M K and Nankali M 2022 A novel temperature-dependent percolation model for the electrical conductivity and piezoresistive sensitivity of carbon nanotube-filled nanocomposites *Acta Mater.* **230** 117870

[34] Aviles F, May-Pat A, Canche-Escamilla G, Rodriguez-Uicab O, Ku-Herrera J J, Duarte-Aranda S, Uribe-Calderon J, Gonzalez-Chi P I, Arronche L and La Saponara V 2016 Influence of carbon nanotube on the piezoresistive behavior of multiwall carbon nanotube/polymer composites *J. Intell. Mater. Syst. Struct.* **27** 92–103

[35] ASTM D638 2014 *Standard Test Method for Tensile Properties of Plastics* (West Conshohocken, PA: American Standard for Testing and Materials)

[36] Blythe T and Bloor D 2005 *Electrical Properties of Polymers* (New York, N Y.: Cambridge University Press)

[37] Otero-Navas I, Arjmand M and Sundararaj U 2017 Carbon nanotube induced double percolation in polymer blends: Morphology, rheology and broadband dielectric properties *Polymer* **114** 122–34

[38] Yu C R, Wu D M, Liu Y, Qiao H, Yu Z Z, Dasari A, Du X S and Mai Y W 2011

Electrical and dielectric properties of polypropylene nanocomposites based on carbon nanotubes and barium titanate nanoparticles *Compos. Sci. Technol.* **71** 1706–12

[39] Meisak D, Macutkevic J, Selskis A, Banys J and Kuzhir P 2020 Dielectric Properties and Electrical Percolation in MnFe2O4/Epoxy Resin Composites *Phys. Status Solidi Appl. Mater. Sci.* **217** 4–9

[40] Pötschke P, Dudkin S M and Alig I 2003 Dielectric spectroscopy on melt processed polycarbonate—multiwalled carbon nanotube composites *Polymer* **44** 5023–30

[41] Samir Z, El Merabet Y, Graça M P F, Teixeira S S, Achour M E and Costa L C 2018 Impedance spectroscopy study of polyester/carbon nanotube composites *Polym. Compos.* **39** 1297–302

[42] Xia X, Zhong Z and Weng G J 2017 Maxwell–Wagner–Sillars mechanism in the frequency dependence of electrical conductivity and dielectric permittivity of graphene-polymer nanocomposites *Mech. Mater.* **109** 42–50

[43] Vertuccio L, Guadagno L, Spinelli G, Lamberti P, Tucci V and Russo S 2016 Piezoresistive properties of resin reinforced with carbon nanotubes for health-monitoring of aircraft primary structures *Compos. Part B Eng.* **107** 192–202

[44] Pérez-Aranda C, Valdez-Nava Z, Gamboa F, Cauich-Rodríguez J V and Avilés F 2020 Electro-mechanical properties of thermoplastic polyurethane films and tubes modified by hybrid carbon nanostructures for pressure sensing *Smart Mater. Struct.* **29** 115021

[45] Bird J 2017 *Electrical and Electronic Principles and Technology* (London, UK.: Routledge)

[46] Mao H, Liu D, Zhang N, Huang T, Kühnert I, Yang J and Wang Y 2020 Constructing a Microcapacitor Network of Carbon Nanotubes in Polymer Blends via Crystallization-Induced Phase Separation Toward High Dielectric Constant and Low Loss *ACS Appl. Mater. Interfaces* **12** 26444–54

[47] Brandrup J, Immergut E H and Grulke E A 2003 *Polymer handbook* vol II (New York, N Y.: Wiley-Interscience)

[48] Nilsson J W and Riedel S 2010 *Electric Circuits* (New Jersey: Prentice Hall Press)

[49] Cen-Puc M, Pool G, Avilés F, May-Pat A, Flores S, Lugo J, Torres G, Gus L, Oliva

A I and Corona J E 2016 A dedicated electric oven for characterization of thermoresistive polymer composites *J. Appl. Res. Technol.* **14** 268–77

[50] Ebbesen T W, Lezec H J, Hiura H, Bennett J W, Ghaemi H F and Thio T 1996 Electrical conductivity of individual carbon nanotubes *Nature* **384** 54–6

[51] Simsek Y, Ozyuzer L, Seyhan A T, Tanoglu M and Schulte K 2007 Temperature dependence of electrical conductivity in double-wall and multi-wall carbon nanotube/polyester nanocomposites *J. Mater. Sci.* **42** 9689–95

[52] Chazot C A C and Hart A J 2019 Understanding and control of interactions between carbon nanotubes and polymers for manufacturing of high-performance composite materials *Compos. Sci. Technol.* **183** 107795

[53] Schawe J E K, Pötschke P and Alig I 2017 Nucleation efficiency of fillers in polymer crystallization studied by fast scanning calorimetry: Carbon nanotubes in polypropylene *Polymer* **116** 160–72

[54] Torres F G and Saavedra A C 2020 A comparison between the failure modes observed in biological and synthetic polymer nanocomposites *Polym. Technol. Mater.* **59** 241–70

[55] Menard K P 2008 *Dynamic Mechanical Analysis* (Boca Raton, FL.: CRC press)

[56] Bartenev G M and Aliguliev R M 1984 Relaxation transitions in polypropylene *Polym. Sci.* **26** 1383–94

[57] Chung D D L 2022 Pitfalls in Piezoresistivity Testing *J. Electron. Mater.* **51** 5473–81